Simultaneous two-photon calcium imaging at different depths with spatiotemporal multiplexing

Adrian Cheng[1–3,5], J Tiago Gonçalves[2,5], Peyman Golshani[2], Katsushi Arisaka[1,4] & Carlos Portera-Cailliau[2,3]

***In vivo* two-photon calcium imaging would benefit from the use of multiple excitation beams to increase scanning speed, signal-to-noise ratio and field of view or to image different axial planes simultaneously. Using spatiotemporal multiplexing we circumvented light-scattering ambiguity inherent to deep-tissue multifocal two-photon microscopy. We demonstrate calcium imaging at multiple axial planes in the intact mouse brain to monitor network activity of ensembles of cortical neurons in three spatial dimensions.**

Optical probing of neuronal activity with fluorescent calcium indicators is a powerful approach to study information processing in the brain[1]. In particular, calcium imaging with two-photon laser scanning microscopy (2PLSM)[2] is an ideal tool for recording network activity *in vivo* because it is less invasive than electrophysiology, more cells can be monitored simultaneously, and one can identify the cells being recorded[3]. Recently, several approaches have been introduced to overcome the traditionally slow raster scanning in two-photon calcium imaging (2PCI), including acousto-optic deflectors (AODs) or targeted path scanning with closed-loop scanning mirrors[4–7]. Thus, as better fluorescent probes and methods for enhancing excitation and detection become available, temporal resolution in 2PCI will improve and reporting of action potential firing will be possible for large groups of neurons in volumes of tissue *in vivo*.

Another way to improve temporal resolution in 2PCI is to scan the sample with multiple beams in parallel[8,9]. In fact, because time resolution, signal-to-noise ratio and field of view are closely related in 2PCI, multifocal scanning would lead to improvements in all of these areas. For instance, in cases for which nonlinear photodamage is a limitation[10], scanning with multiple beams simultaneously and increasing the rate at which laser pulses are delivered to the sample will increase the signal-to-noise ratio[11]. Another potential

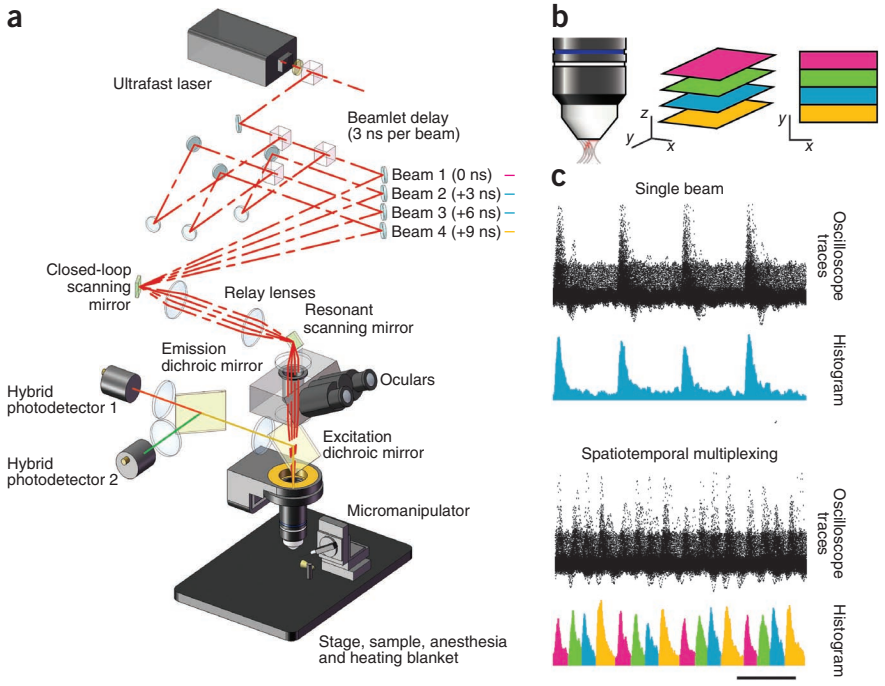

Figure 1 | Spatiotemporal multiplexing to overcome depth limitations in multifocal 2PLSM. (**a**) Layout of the prototype microscope. Laser pulses are emitted with a 12-ns period from a commercial ultrafast Ti:Al_2O_3 laser. The beam is divided into four beams, which are delayed by 3 ns each (1 m per 3 ns) and converged on the slow-axis scan mirror aperture, which is then projected onto the objective back aperture. The resulting emitted fluorescence, which is highly scattered, is collected by two hybrid photodetectors. The hybrid photodetector's active area is placed in a demagnified conjugate plane of the objective back aperture to maximize scattered light collection. (**b**) Schematic of different beam-scanning patterns at the sample. Time multiplexing removes ambiguity between different imaging planes, allowing both axial and lateral beam distribution. (**c**) Time course of detected fluorescence signal for a single beam (top) and four spatiotemporally multiplexed beams (bottom). Overlay of 200 oscilloscope traces and summary histograms of single photoelectron events (using a pollen grain). Fluorescence from different time windows (different colors) is associated with different delayed excitation beams. Scale bar, 12 ns.

[1]Department of Physics and Astronomy, University of California Los Angeles, Los Angeles, California, USA. [2]Department of Neurology, David Geffen School of Medicine, University of California Los Angeles, Los Angeles, California, USA. [3]Department of Neurobiology, David Geffen School of Medicine, University of California Los Angeles, Los Angeles, California, USA. [4]California NanoSystems Institute,University of California, Los Angeles, Los Angeles, California, USA. [5]These authors contributed equally to this work. Correspondence should be addressed to C.P.-C. (cpcailliau@mednet.ucla.edu).

RECEIVED 1 OCTOBER 2010; ACCEPTED 14 DECEMBER 2010; PUBLISHED ONLINE 9 JANUARY 2011; DOI:10.1038/NMETH.1552

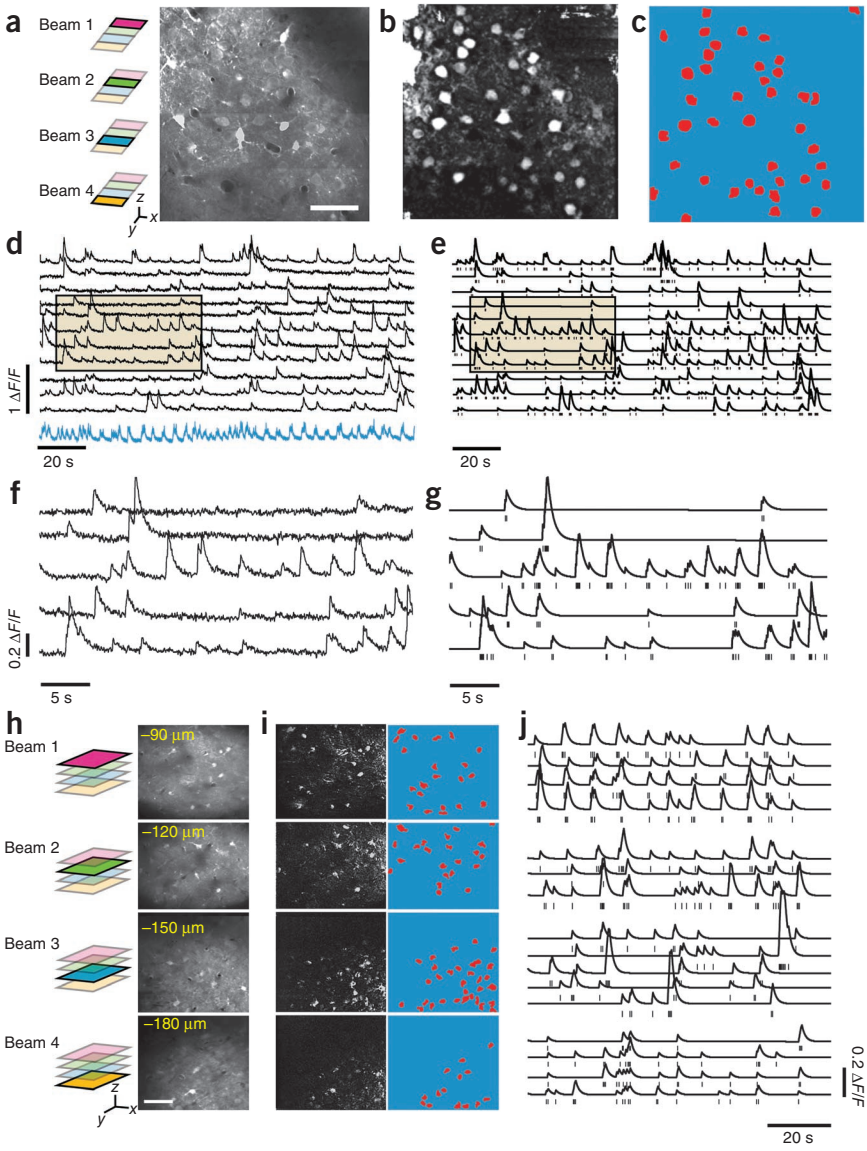

Figure 2 | Multifocal two- and three-dimension *in vivo* 2PCI of L2/3 neurons in barrel cortex with spatiotemporal multiplexing. (**a**) Spatial distribution of four beams in a single image plane (left) and typical field of view (right), an average intensity time projection of a representative calcium imaging movie (3 min, 250 frames s^{-1}) from a P20 mouse using Fluo-4 AM. Scale bar, 50 µm. (**b**) Zero-lag cross-correlation image computed from a movie. (**c**) Final segmented image of cell bodies obtained through morphological filters (red contours). (**d**) Raw calcium traces of 11 different cells (neurophil signal in blue). (**e**) Model calcium traces with identified neuronal spiking events (tic marks) of selected cells using a peeling algorithm are shown with relative fluorescence change ($\Delta F/F$). (**f**,**g**) Details of shaded regions shown in **d** and **e**, respectively. (**h**) Spatial distribution of four beams arranged axially (left) and field of view for each imaging plane (right). Images are average intensity time projections of a typical movie with Fluo-4 AM (3 min, 60 volumes s^{-1}) with depth spanning from 90 µm to 180 µm below the pia (encompassing layers 1 to 3). Scale bar, 50 µm. (**i**) Zero-lag cross-correlation image (left) and fully segmented image (right) with cell contours (red). (**j**) Selected traces reconstructed by the peeling algorithm, with rows in **i** and **j** corresponding to beams shown in **h**.

advantage of multifocal 2PLSM would be the capability to perform calcium imaging of multiple axial planes simultaneously.

Because the brain is a heterogeneous medium that greatly scatters and absorbs light, multifocal 2PCI in the intact brain has not yet been feasible at depths greater than 100 µm. The deep-tissue imaging capability of 2PLSM requires non-descanned detection of scattered fluorescence[2], relying solely on excitation for spatial contrast. Existing commercial multifocal 2PLSM systems use cameras that generate spatial contrast through detection[8], which is subject to much greater scattering than excitation for a given depth[12]. This leads to a substantial loss of spatial resolution and signal strength with depth (**Supplementary Fig. 1**). The use of descanned detector arrays such as multianode photomultiplier tubes can decrease this effect[9], but this method is still subject to scattering ambiguity in the form of emission crosstalk and is limited to less than 70 µm tissue penetration.

A solution to the problem of extending multifocal raster scanning with 2PLSM to deep tissue is to use spatiotemporal excitation pulse multiplexing and demultiplexed readout[13]. The feasibility of this approach to image fluorescent samples at multiple focal planes has been demonstrated with custom lasers[13–15]. It has been hypothesized that this method would allow multiple beams to be used in deep tissue without scattering ambiguity[14]. Here we adopted this approach for 2PCI *in vivo* using traditional non-descanned detection to collect all scattered light and attribute it to individual beams. We demonstrate that this technique can be applied to achieve multifocal 2PCI in the intact mouse neocortex, at depths greater than the visible wavelength mean free path length and in multiple axial planes across several cortical layers.

Our multifocal 2PCI approach takes advantage of the shorter fluorescence decay time of synthetic fluorescent calcium indicator dyes (typically in the nanosecond range) relative to the laser repetition periods (tens of nanoseconds) to interleave beams in time. This permits fluorescence from spatially distinct beams to be distinguished because fluorescence detected at different times is assigned to different portions of the image (**Fig. 1**). The number of beams that can be implemented is ultimately determined by the laser repetition rate and the fluorophore's decay time. Using a standard 80-MHz Ti:Al_2O_3 laser, this translates into simultaneously scanning four beams that are separated in time by ~3 ns, which works well for the commonly used dye Fluo-4 (~1 ns lifetime; **Supplementary Note 1**). Many more beams could be added (and more fluorophores accommodated) by using methods to reduce the repetition rate of commercial lasers (**Supplementary Note 1**). To achieve short beam spacing and analog readout, we used a prototype hybrid photodetector[16] with a short single-photoelectron pulse width and transit time spread (Online Methods). Nevertheless, a variety of detection schemes could be used[15].

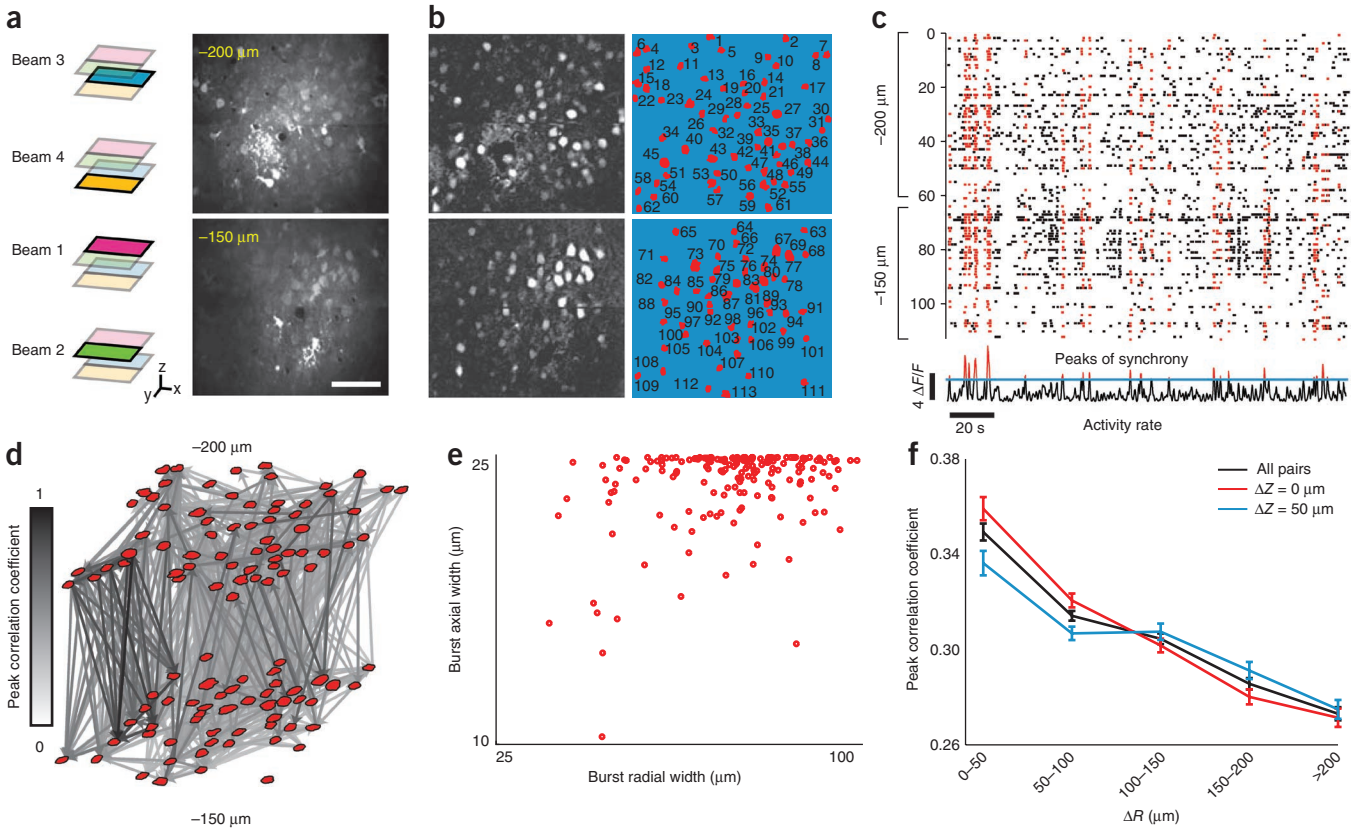

Figure 3 | Multifocal 2PCI with spatiotemporal multiplexing to assess activity-derived neuronal connectivity in L2/3 of barrel cortex. (**a**) Spatial distribution of four scanning beams (left) and representative field of view in two separate imaging planes (right) from an experiment with a P20 mouse using Fluo-4 AM (3 min, 100 frames s^{-1}). Scale bar, 50 µm. (**b**) Zero-lag cross-correlation image (left) and segmented image (right) of the same experiment, with rows in **a** corresponding to rows in **b**. Cells are numerically ordered according to their vertical coordinates. (**c**) Raster plot showing identified spiking events in cells from **b**. Events shown in red were identified as having participated in a peak of synchrony (bottom trace). (**d**) Peak correlation coefficient (over a time lag of ± 1 s) for significantly correlated ($P < 0.05$; as defined in Online Methods) cells shown in **b**. (**e**) Axial (depth) versus radial (lateral) spread of bursts of neuronal firing corresponding to peaks of synchrony identified in several movies (10 movies from 2 mice, 173 peaks of synchrony). A minority of bursts had a spatial organization consistent with either columnar (top left) or laminar connectivity (bottom right). (**f**) Peak correlation coefficients from **c** versus cell pair radial distance (ΔR), for cell pairs in different imaging planes, the same imaging plane and for all pairs (10 movies, 10,262 pairs). Error bars, s.e.m.

To test whether multifocal 2PLSM with excitation-emission multiplexing can be used for calcium imaging in the intact brain, we combined our four-beam system with a resonant scanning mirror (although any scanning method could be used; **Supplementary Note 1**). This allows acquisition of two-dimensional images with 500 × 500–pixel resolution at up to 250 Hz, corresponding to a maximum field of view of ~400 × 400 µm using a 40× objective (**Figs. 2** and **3** and **Supplementary Fig. 2**). We used standard Fluo-4 acetoxymethyl ester (AM) bulk-loading protocols to record the activity of layer 2/3 (L2/3) neurons in the somatosensory cortex of isoflurane-anesthetized mice. To identify cell contours for analysis, we used a morphological analysis of the time-dimension zero-lag cross-correlation image (**Fig.2b** and Online Methods). For iterative identification of action potential–dependent calcium transients in neurons, we used a 'peeling algorithm'[7]; Online Methods) and constructed raster plots of discrete neuronal firing events (**Fig. 2**). Simultaneous patch-clamp recordings in cell-attached mode showed that the simulated calcium traces convolved from the electrophysiology recordings closely resembled the actual calcium traces (**Supplementary Fig. 2**). Thus, our prototype four-beam time-multiplexed microscope performed well for *in vivo* 2PCI of the activity of L2/3 neurons and provided the expected 4× larger field of view (or 4× greater time resolution) than conventional single-beam 2PLSM systems.

A current limitation of 2PCI is that one cannot easily record network activity at different depths simultaneously. Using AODs with chirped acoustic signals, one can achieve inertia-less random-access axial focusing at kilohertz rates. However, 2PCI in multiple depths with AODs has only been demonstrated in brain slices with a modest ± 25 µm range[6]. The approach also requires four AODs, which introduces considerable optical losses as well as detrimental temporal and spatial dispersion. An alternative is to use a piezoelectric objective focusing unit to rapidly move the objective lens[5], which allows volumes to be scanned at rates of ~10 Hz, but the approach is ultimately inertia-limited. Neither method captures full imaging data, precluding the use of image-registration methods for motion correction or image-processing algorithms for cell detection a posteriori.

To image calcium signals in three dimensions with spatiotemporal multiplexing, we implemented slight modifications in the optics of our system to scan separate imaging planes with different beams (**Supplementary Fig. 3**). We arranged beams quasi-collinearly with

a lens added for each beam to allow for focus offset in the axial direction while maintaining uniform back-aperture filling. We spaced the beams 30 µm apart from each other in the *z* axis for a total pitch of 90 µm. The total axial spacing was ultimately limited by spherical aberration of the objective lens (**Supplementary Note 1**). This allowed us to monitor the activity of ~100–200 neurons distributed over a cortical volume spanning from layer 1 to layer 3 (**Fig. 2h–j**).

To test potential applications of multifocal 2PLSM with spatiotemporal multiplexing, we conducted 2PCI experiments at multiple axial depths to determine whether spontaneous activity in L2/3 of barrel cortex can spread in a columnar fashion, as previously reported[17]. We recorded neuronal activity with Fluo-4 AM in postnatal day 15–21 (P15–P21) anesthetized mice. To maximize the number of L2/3 cells imaged, we arranged the beams such that only two planes (spaced at 50 µm pitch) were imaged simultaneously, each with two beams (**Fig. 3**). Next, we identified cells that participated in synchronous bursts of activity, previously referred to as peaks of synchrony[17] (Online Methods). We also constructed activity-derived connectivity diagrams and plotted the distribution of peak correlation coefficients among pairs of cells in separate depths in L2/3 (**Fig. 3d**). We found that only a minority of these bursts had an axial (depth) and radial (lateral) spread that would be consistent with columnar connectivity (**Fig. 3e**), and the relationship between peak correlation coefficient and the axial spread (ΔR) of a cell pair was indistinguishable for cells in the same imaging plane or in different planes (**Fig. 3f**). These data suggest that spontaneous activity in L2/3 does not tend to propagate along columnar boundaries.

Ideally, one would like to introduce more than four beams and accommodate a wider variety of fluorophores, including those with longer lifetimes. The simplest solution is to use a laser with a lower repetition rate while conserving average power (**Supplementary Note 1**). In practice, to use a range of fluorescent dyes, beams should be spaced on the order of 10 ns apart, giving a maximum sample pulse rate and pixel rate of 100 MHz. This is a maximum rate at which information can be extracted by fluorescence emission from a region over which the returning fluorescence is scattered and diffused. Ultimately, the pulse energy required depends on tissue scattering, depth, wavelength, pulse width, focus quality, overall system optical transmission, nonlinear photodamage and the fluorophore of interest; in our case, a pulse energy of 0.1–1 nJ after the objective lens was sufficient for *in vivo* 2PCI. Therefore, using a 5-MHz laser with ~2–3 W average power at 800 nm, imaging with 8–16 beams should be feasible for a wide variety of commonly used fluorophores.

Here we applied a spatiotemporal multiplexing technique to address the fundamental limitation of deep tissue scattering ambiguity in multifocal 2PLSM. In the future, the introduction of additional beams and greater axial pitch will make it possible to record activity from an entire volume of neocortex. Additionally, multifocal 2PLSM with time multiplexing could be combined with AOD scanning or targeted path scanning (**Supplementary Note 1**). In parallel with improvements in excitation efficiency, electronics, light collection and detectors that result in higher signal-to-noise ratio, multifocal 2PCI with multiplexing will allow neuroscientists to explore new questions regarding the spatiotemporal dynamics of neuronal activity over three spatial dimensions.

METHODS

Methods and any associated references are available in the online version of the paper at http://www.nature.com/naturemethods/.

Note: Supplementary information is available on the Nature Methods website.

ACKNOWLEDGMENTS

We thank D. Kleinfeld, J.F. Léger, T. Otis and members of the Portera-Cailliau laboratory for discussions and comments on the manuscript, and M. Suyama and Y. Kawai (Hamamatsu Photonics K.K.) for engineering support. This work was supported by grants from the US National Institutes of Health (the Eunice Kennedy Shriver National Institute of Child Health and Human Development, the National Institute of Neurological Disorders and Stroke) and the US National Science Foundation (Major Research Instrumentation Program).

AUTHOR CONTRIBUTIONS

A.C., J.T.G., P.G., K.A. and C.P.-C. conceived the project. A.C. designed and built the microscope and control electronics, and developed the microscope software. J.T.G. performed *in vivo* multifocal calcium imaging and simultaneous cell-attached recordings. A.C. analyzed the data. A.C., J.T.G. and C.P.-C. wrote the manuscript. K.A. and C.P.-C. supervised the project.

COMPETING FINANCIAL INTERESTS

The authors declare no competing financial interests.

Published online at http://www.nature.com/naturemethods/.
Reprints and permissions information is available online at http://npg.nature.com/reprintsandpermissions/.

1. Grewe, B.F. & Helmchen, F. *Curr. Opin. Neurobiol.* **18**, 520–529 (2009).
2. Svoboda, K. & Yasuda, R. *Neuron* **50**, 823–839 (2006).
3. Kerlin, A.M., Andermann, M.L., Berezovskii, V.K. & Reid, R.C. *Neuron* **67**, 858–871 (2010).
4. Kremer, Y. *et al. Opt. Express* **16**, 10066–10076 (2008).
5. Gobel, W., Kampa, B.M. & Helmchen, F. *Nat. Methods* **4**, 73–79 (2007).
6. Duemani Reddy, G., Kelleher, K., Fink, R. & Saggau, P. *Nat. Neurosci.* **11**, 713–720 (2008).
7. Grewe, B.F., Langer, D., Kasper, H., Kampa, B.M. & Helmchen, F. *Nat. Methods* **7**, 399–405 (2010).
8. Nielsen, T., Fricke, M., Hellweg, D. & Andresen, P. *J. Microsc.* **201**, 368–376 (2001).
9. Kim, H. *et al. Opt. Express* **15**, 11658–11678 (2007).
10. Hopt, A. & Neher, E. *Biophys. J.* **80**, 2029–2036 (2001).
11. Ji, N., Magee, J.C. & Betzig, E. *Nat. Methods* **5**, 197–202 (2008).
12. Oheim, M., Beaurepaire, E., Chaigneau, E., Mertz, J. & Charpak, S. *J. Neurosci. Methods* **111**, 29–37 (2001).
13. Amir, W. *et al. Opt. Lett.* **32**, 1731–1733 (2007).
14. Sheetz, K.E., Hoover, E.E., Carriles, R., Kleinfeld, D. & Squier, J.A. *Opt. Express* **16**, 17574–17584 (2008).
15. Chandler, E. *et al. Appl. Opt.* **48**, 2067–2077 (2009).
16. Michalet, X. *et al. Proc. SPIE* **6862**, 0F1–0F12 (2008).
17. Cossart, R., Aronov, D. & Yuste, R. *Nature* **423**, 283–288 (2003).

ONLINE METHODS

Reagents and animals. All chemicals were purchased from Sigma-Aldrich unless otherwise stated. All experiments were performed under animal protocols approved by the Animal Research Committee and the Office for the Protection of Research Subjects at the University of California, Los Angeles.

Spatiotemporal beam multiplexing. To construct the spatiotemporal beam multiplexing microscope prototype (**Fig. 1a**), we used simple optics to split the main beam from a 80 MHz Ti:Al_2O_3 laser (Chameleon Ultra II, Coherent) into four spatiotemporally multiplexed beams. Polarizing beam splitters were used with half-wave plates to allow for varying power delivery via each beam. We calculated that, for a 3 ns delay between beams, each beam's path had to be extended by a distance of ~1 m. The delayed beams were then converged on a conjugate plane of the objective pupil at the desired angle. Differences in optical propagation time of emitted fluorescence owing to each beam were deemed negligible because of the short differences in distance traveled (millimeters) compared to the optical delays (meters). During fluorescence emission from each beam, the photodetector remains sensitive to the entire collection area of the objective, which ensures that the sensitivity and resolution are equivalent to those of a single beam system.

Pulse length is degraded by group delay dispersion and, as determined by previous work[18] and by the Sellmeier equation, this is negligible for the optical train consisting of ~1 m air delay lines using several dielectric mirrors. The dominant contribution from delay lines is from dielectric mirrors (~20 fs^2 at 800 nm[18]). In the overall microscope system the largest contributors to group delay dispersion were the glass elements (506 fs^2 cm^{-1} for BK7 glass at 800 nm, 594 fs^2 cm^{-1} for LakL21 at 800 nm), and in comparison delay line dispersion was negligible.

For imaging different planes simultaneously, the beams were arranged quasi-collinearly with a lens added for each beam to allow for focus offset in the axial direction while maintaining uniform back aperture filling (**Supplementary Fig. 3**). Beams were spaced either 30 µm apart in the *z* axis (for a total pitch of 90 µm) under 40× magnification in the case of four plane experiments (**Fig. 2**), 75 µm apart in the case of two plane experiments under 40× magnification, or 50 µm apart under 60× magnification (**Fig. 3**).

De-multiplexing fluorescence emission. To de-multiplex fluorescence emission, we chose a state-of-the-art hybrid photodetector (HPD; Hamamatsu Photonics), which uses an avalanche photodiode as an electron bombardment target instead of the dynode stages of a photomultiplier tube (PMT). The HPD has a high first stage electron bombardment gain, which allows a low excess noise factor (a measure of the charge fluctuation of each single photoelectron response) of ~1.3, as well as a high speed response (<1 ns) that is limited by the capacitance of the target avalanche photodiode[19]. Although the HPD's single photoelectron gain of approximately 10^5 is an order of magnitude lower than that of a PMT, the difference is recovered with a gigahertz preamplifier (**Supplementary Fig. 4**). The HPD we used had a GaAsP photocathode with a 3-mm-diameter active area and 45% quantum efficiency at 510 nm. A custom circuit board was designed and fabricated to demodulate multiplexed signals, built around an analog multiplier integrated circuit (ADL5391, Analog Devices). Emission signals from the HPD were de-multiplexed by analog multiplication with 3-ns square pulses generated from the laser monitor signal. This resulted in four separate signals that were shaped and amplified for subsequent digitization. Thus, our prototype system could operate as a fluorescence lifetime imaging system when used with a single excitation beam, using 3-ns-wide gates in the time domain.

Laser scanning system, image display and storage. For calcium imaging with our prototype four-beam system, we incorporated either a 16-kHz resonant scanning mirror (SC-30, EOPC) or a 12-kHz resonant scanning mirror (CRS, Cambridge Technology/GSI Lumonics). This is a conventional scan method that has been used previously for 2PLSM[20–22]. The resonant scanning mirror executes a bidirectional sinusoidal scan, producing a line rate of 32 kHz or 24 kHz, respectively. We compensated for the non-uniform power delivery per angle and depth with an electro-optic modulator (S-350, ConOptics), but one could instead block the edges of the scan range. For the slow scan axis, we used a closed-loop scanning mirror (6200H, Cambridge Technology). Function generators were used to generate scanning mirror signals (33210A, Agilent). With these components, our four-beam system is capable of acquisition rates of up to 250 frames s^{-1} with for 512 × 512 images for single plane imaging and 60 volumes s^{-1} for multiple plane imaging.

After de-multiplexing and amplification, signals were digitized by a standard four-channel frame-grabber acquisition board (Helios, Matrox; **Supplementary Fig. 4**). Using two HPDs and a fast analog switch (ZYSW-two-50DR, Mini-Circuits), two colors can be switched or interleaved at the pixel or frame level and digitized by the same board. Signals were digitized at 8-bit precision per sample at 80 MHz, using a clock signal derived from the laser. We did not use the HPD in a photon-counting readout scheme to allow for high peak photon flux, but this is certainly possible. Once digitized, the data were transferred across the peripheral bus at sustained transfer rates >700 megabytes per second (MB s^{-1}) and then displayed in real time by custom software using supplied imaging libraries (Matrox Imaging Library, Matrox). Raw images were averaged for display purposes only (to help visualize Fluo-4–labeled cells), while complete raw data was stored on hard disk. Geometrical horizontal distortion owing to sinusoidal scanning distortion was corrected offline by linear interpolation resampling or online with nearest-neighbor resampling. Imaging data were stored across a custom-designed high-bandwidth hard disk array with a maximum sustained transfer rate of 400 MB s^{-1} (Windows XP; Microsoft). This allows for two channels of data to be recorded without interruption at roughly 100 MB s^{-1} at 10-bit resolution. Data can be continuously recorded until the disk array space is exhausted (~3 h).

***In vivo* cranial window preparation, calcium dye injection and imaging.** We used male and female juvenile c57Bl/6 mice (12 mice; postnatal days 15–21) for all experiments and followed standard protocols[23–25]. A modified cranial window surgery, in which the glass coverslip only partially covers the dura, leaving a gap for injecting the calcium indicator was performed under isoflurane anesthesia (1.5% in O_2). Sulforhodamine 101 was also injected to label astrocytes. With 2–4 injections of the calcium dye per mouse, we could label thousands of L2/3 neurons

over a large area (1 mm^2). We started 2PCI at 800 nm of Fluo-4 AM or Oregon green BAPTA-1 AM (OGB) after a 30–60 min recovery period. We used three different objectives: 40× 1.0 numerical aperture (NA) (Zeiss), 40× 0.8 NA (Olympus) and 60× 0.9 NA (Olympus). Typically, an average power of 1 W at 800 nm was input into the microscope (**Supplementary Fig. 5**). The emission of sulforhodamine 101 in the red channel (filter, 629/53 nm) was separated from that of the calcium dye in a green channel (filter, 525/50 nm) with a dichroic that transmits wavelengths above 562 nm. Calcium imaging was done while mice were under isoflurane anesthesia (~0.5–1%). Several 180 s image sequences were recorded (250 frames s^{-1} with 16 kHz resonant scanning mirror and single imaging plane; 60 volumes s^{-1} for four-plane imaging; and 100 volumes s^{-1} for two-plane imaging with 12 kHz resonant scanning mirror). For multiple plane imaging, individual beam powers were carefully adjusted by half-wave plates and polarizing beam splitters to compensate for varying depth of imaging and variations in preparations. Beam crosstalk owing to fluorescence lifetime was deemed negligible (**Supplementary Figs. 6** and **7**), and no losses owing to multiple beam imaging were found (**Supplementary Fig. 8**).

Electrophysiological recordings. *In vivo* loose cell-attached recordings were performed as previously described[26], using a patch clamp amplifier (2400, A-M Systems) and borosilicate microelectrodes (4–6 MΩ) filled with a potassium gluconate solution containing 105 mM K-gluconate, 30 mM KCl, 10 mM HEPES, 10 mM phosphocreatine, 4 mM ATP-Mg, 0.3 mM GTP (adjusted to pH 7.3 with KOH). Cells were targeted using the shadow-patch method[27].

Image processing and data analysis. Image processing was done using the Matlab environment (MathWorks). Images were first transformed using linear interpolation to correct for the sinusoidal resonant scanner trajectory. Contours of cells were detected by generating an image of the zero-lag cross correlation (or normalized standard inner product) between a 1 μm neighborhood and a 10 μm neighborhood[28,29]. The resulting image was thresholded to generate cell contours. Once cells were identified, raw fluorescence intensity traces were calculated for each, and linear drift was then subtracted. A peeling algorithm[30] was applied to identify transients by procedurally fitting exponentials with fixed decay length of 1 s and amplitude at least 5% relative fluorescence change ($\Delta F/F$) using linear least-squares method, accepting fits with average R^2 improvement greater than 0.1 s.d. over the mean. After each successful fit, the detected transient was subtracted from the data and another fit was attempted, until the end of the trace was reached. This resulted in lists of events, their amplitude and times for each cell.

To identify peaks of synchrony, the event-amplitude was summed over all cells and a trigger was applied over time at a threshold determined by Monte Carlo analysis (1,000 simulations), as previously described[31]. This consisted of generating Monte Carlo datasets assuming uniform event arrival time while preserving the event amplitude distribution and number and then identifying the 95% confidence limit (CL) threshold for peak total event amplitude per time. Once peaks of synchrony were identified, the spatial distribution of the cells participating in each peak was characterized using the s.d. of cell position in the radial (that is, lateral) and axial directions. To identify significantly correlated cell pairs ($P < 0.05$), the peak of the cross-correlation function between event rates for pairs of cells was calculated, as was the delay time at which the peak occurred (with a maximum amplitude of 1 s). Monte Carlo analysis involving 1,000 trials of randomly permuting of event times was performed to identify 95% CL thresholds for peak cross-correlation values for each cell pair.

18. Beck, M., Walmsley, I.A. & Kafka, J.D. *IEEE J. Quantum Elect.* **27**, 2074–2081 (1991).
19. Fukasawa, A.J. *et al. IEEE Trans. Nuclear Sci.* **55**, 758–762 (2008).
20. Sanderson, M.J. & Parker, I. *Methods Enzymol.* **360**, 447–481 (2003).
21. Fan, G.Y. *et al. Biophys. J.* **76**, 2412–2420 (1999).
22. Rochefort, N.L. *et al. Proc. Natl. Acad. Sci. USA* **106**, 15049–15054 (2009).
23. Mostany, R. & Portera-Cailliau, C. *J. Vis. Exp.* published online 15 February 2008 (doi:10.3791/680).
24. Golshani, P. & Portera-Cailliau, C. *J. Vis. Exp.* published online 13 March 2008 (doi:10.3791/681).
25. Garaschuk, O., Milos, R.I. & Konnerth, A. *Nat. Protoc.* **1**, 380–386 (2006).
26. Golshani, P. *et al. J. Neurosci.* **29**, 10890–10899 (2009).
27. Kitamura, K., Judkewitz, B., Kano, M., Denk, W. & Hausser, M. *Nat. Methods* **5**, 61–67 (2008).
28. Smith, S.L. & Hausser, M. *Nat. Neurosci.* **13**, 1144–1149 (2010).
29. Valmianski, I. *et al. J. Neurophysiol.* **104**, 1803–1822 (2010).
30. Grewe, B.F., Langer, D., Kasper, H., Kampa, B.M. & Helmchen, F. *Nat. Methods* **7**, 399–405 (2010).
31. Cossart, R., Aronov, D. & Yuste, R. *Nature* **423**, 283–288 (2003).

doi:10.1038/nmeth.1552